The Peak Flux Constraints on Bladed Receiver Performance in High-Temperature Molten Salt Concentrating Solar Power Systems

Ye Wang, John Pye

Solar Thermal Group, Research School of Engineering, The Australian National University, Canberra, Australia

E-mail: ye.wang@anu.edu.au

Abstract

Bladed receivers, obtained by rearranging the tube-banks of conventional convex tubular receivers, may offer the potential to improve performance and increase efficiency for concentration solar power (CSP) systems. With smaller aperture and higher concentration ratio, bladed receivers will dramatically decrease reflection and re-radiation losses. But the minimum receiver area is also limited by the constraint of the peak flux limitation on stability of molten salt and tube stresses, which is around 850–1000 suns. Under this constraint, we evaluate on a flat receiver and a range of different sizes of bladed receivers. We keep the same peak flux limitation (800 suns) and same total incident irradiance, but a real flux distribution for each case from ray-tracing simulations. The Monte-Carlo Ray Tracing (MCRT) method is used to calculate the radiative thermal emissions from each surface, for surface temperature distributions capable with the thermal limits of molten salt heat transfer fluid. Results shown that bladed receivers have the capacity to work with higher concentration ratio, improving both optical and thermal efficiency while maintaining the peak flux within limits.

1.   Introduction

Tubular receivers are commonly used in large central solar power systems, like Gemasolar, Solar One and Solar Two (Ho et al., 2014). They are composed of banks of tubes arranged over the external surface of a cylinder or a rectangular cuboid. Reflection and re-radiation losses and peak flux limitations are the dominant constraints for this type of receiver in high-temperature molten salt utilizations. One possible approach to improve performance is to re-configure the tubes into bladed shapes, promising cavity-like benefits for light trapping (Wang et al., 2016). The bladed receiver will have a smaller aperture than an equal-area flat tubular receiver. Also, based on the assumption that both receivers have the same total incident irradiance uniformly distributed over the isothermal surfaces, a first-order analysis showed that bladed receivers can be designed to be simultaneously lighter and more efficient (Pye et al., 2016).

A smaller aperture with a higher concentration ratio will dramatically decrease reflection and re-radiation losses, but the minimum receiver area is also limited by the constraint of the peak flux limitation (around 850–1000 suns for molten salt) (Falcone, 1986 and Pye et al., 2016). Excessive flux can easily cause tube or working fluid temperature limit to be exceeded (Kolb, 2011).

In this study, we address the challenge of maintaining peak flux within limits on stability of molten salt and tube stresses. We improve upon the first-order theoretical analysis previously presented (Pye et al., 2016). We evaluate a flat receiver and compare with bladed receivers with a range of different sizes, in both cases subject to the same peak flux limitation (800 suns), the same total incident irradiance, but a real flux distribution for each case from ray-tracing simulations.

The Monte-Carlo Ray Tracing (MCRT) method is used to calculate the radiative thermal emissions from each surface, for surface temperature distributions capable with the thermal limits of molten salt heat transfer fluid. We analyze the thermal efficiency and overall receiver efficiency under different concentration ratios. The research methods and results are discussed in the following sections.

2.   Methods

Optical and thermal (specifically, radiative thermal emissions) performance of bladed receivers are evaluated and compared with a reference flat receiver.

The constraints applied in their comparison are equal total incident energy and equal peak flux on the tubes. The peak flux is 800 suns, due to thermal stability of molten salt. These constraints are given by Eq. (1) and (2), where 'f' refers to flat receivers and 'b' refers to bladed receivers:

$$\dot{Q}_{inc,f} = \dot{Q}_{inc,b} \tag{1}$$

$$\Phi_{f,max} = \Phi_{b,max} = 800 \text{ kW/m}^2 \tag{2}$$

A bladed receiver will have a smaller aperture than a flat receiver (Pye et al., 2016), so correspondingly higher concentration ratio from the heliostat field is required. One approach to achieve this is using different heliostat fields and adjusting aiming strategies. This approach is highly computationally intensive when dealing with large receiver optimisations, because not only the structure of the receiver is variable, but also the field layout and aiming strategies also need to be designed and optimised. An alternative and computationally cheaper approach is using a heliostat field with flat mirrors and a single aim point. Firstly, we believe that flat heliostats provide the same angular distribution of rays as curved heliostats, which will keep the same flux (positions) distribution on the target, so that we can exam the flux distribution on flat receivers and bladed receivers. We can later apply scaling factors to convert the lower density from flat heliostats to a real value that curved heliostats can provide. Secondly, the single aim point is a proxy to achieve a uniform flux profile on a vertical plane, instead of assuming curved heliostats with a sophisticated aiming strategy. Thirdly, keeping one heliostat field can make sure that the same amount of incident energy comes to the receiver and keeping the same size of the back wall of both bladed and flat receivers can achieve same spillage level. Finally, the peak flux can be scaled up to 800 suns by shrinking down the size of the receiver proportionally and scaling relevant results accordingly. The calculation for this scaling method is shown below.

Figure 1 illustrates the relation between the simulated receivers and the real receivers for performance comparison. 'Real' means that they are working with curved heliostat fields, comparing to the simulated receivers which are mounted on a flat heliostat field that is not true in reality.

We use National Solar Thermal Test Facility (NSTTF) (Yellowhair et al., 2014) with flat mirrors as the simulated heliostat field and the same back wall size (10 m by 10 m) for all of
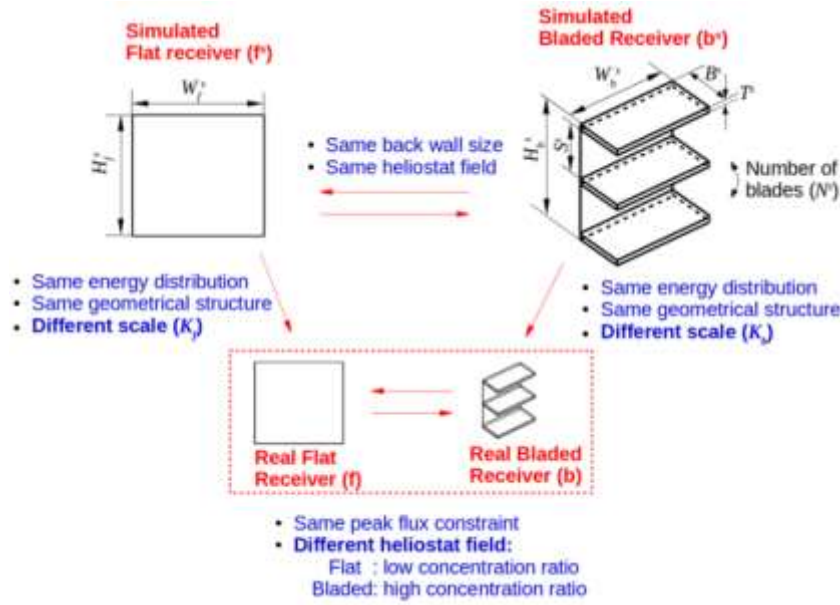
Figure 1. Relation between the simulated model and the real model

the simulated receivers, that is:

$$W_f^s = W_b^s = W^s = 10 \text{ m}$$
$$H_f^s = H_b^s = H^s = 10 \text{ m}$$
(3)

Before applying Monte-Carlo Ray-Tracing (MCRT) simulations, each investigated surface is separated into a rectangular mesh of elements to store the number of randomly generated rays arriving at the corresponding local surface. This is actually the flux distribution. We keep the element size equally for all of the simulated receivers, that is:

$$A_{ij}^s = 0.2 \times 0.2 \text{ m}^2$$
(4)

For the flat receiver, we change the inclination angle of the plane to find the best position to achieve the highest energy absorption. Through ray-tracing simulation, flux distribution and peak flux can be obtained.

The real flat receiver has the same number of elements as the simulated flat receiver, and same amount of energy to be absorbed on the individual element, but the peak flux of the real one is 800 suns. This means that the element size on the real receiver will be different with the simulated one, the relation is:

$$A_{ij}^s \cdot \Phi_{f,max}^s = A_{ij} \cdot \Phi_{f,max}$$
(5)

where A_{ij}^s and A_{ij} are the element area for the simulated case and the real case respectively. Hence the geometrical scaling factor $K_f(<1)$ can be defined as:

$$K_f = \sqrt{\frac{A_{ij}}{A_{ij}^s}} = \sqrt{\frac{\Phi_{f,max}^s}{\Phi_{f,max}}}$$
(6)

The size of the real flat receiver can be obtained as Eq.(7), since all dimensions scale equally.

$$W_f = K_f \cdot W^s$$
$$H_f = K_f \cdot H^s$$
(7)

The flux distribution for the real flat receiver can be scaled correspondingly as Eq. (8), from Eq. (5) and (6).

$$\Phi_{f,ij} = \frac{\Phi_{f,ij}^s}{K_f^2}$$ (8)

For the bladed receiver, it is the same scaling method. The real bladed receiver has the same geometrical structure as the simulated bladed receiver and the same number of elements on each surface. The geometrical scaling factor $K_b(<1)$ for bladed receiver is:

$$K_b = \sqrt{\frac{\Phi_{b,max}^s}{\Phi_{b,max}}}$$ (9)

The scaling and parameter relationship for the real bladed receiver are listed in Table 1.

Table 1. Relations between the real bladed receiver and the simulated receiver

Width	$W = K_b \cdot W^s$	Number of blades	$N = N^s$
Height	$H = K_b \cdot H^s$	Blade angle	$\beta = \beta^s$
Depth	$B = K_b \cdot B^s$	Back wall angle	$\theta = \theta^s$
Thickness	$T = K_b \cdot T^s$	Flux	$\Phi_{b,ij} = \Phi_{b,ij}^s / K_b^2$

The bladed receivers are simulated through varying the depth (B), number of blades(N) and the angles(β and θ). The definition of the angles is in Figure 2, where β is the blade inclination angle (angle between the blade and the back wall),θ is the back wall inclination angle (angle between the back wall and the vertical axis), and φ is the angle between the blade and the vertical axis, which points the direction of blades toward to the field. The relation between them is:

$$\theta = \beta - \varphi$$ (10)
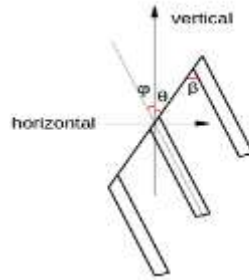
Figure 2. Definition of the angles of bladed receiver

The investigation procedure can be summarised as shown in Fig.3. The optical and thermal model are described in the following sections.

2.1. *Optical Model*

The optical study is performed by ray-tracing simulations using Tracer, a tool that has been introduced in detail in Wang et al., 2016, where flux distribution, optical efficiency,η_{opt}, total incident energy from field to receiver,$\dot{Q}_{inc}$, absorbed energy by the receiver,$\dot{Q}_{abs}$, spillage, $\dot{Q}_{spil}$, and reflection,$\dot{Q}_{refl}$, can be obtained. The optical efficiency is defined as:

$$\eta_{opt} = \frac{\dot{Q}_{abs}}{\dot{Q}_{inc}}$$ (11)
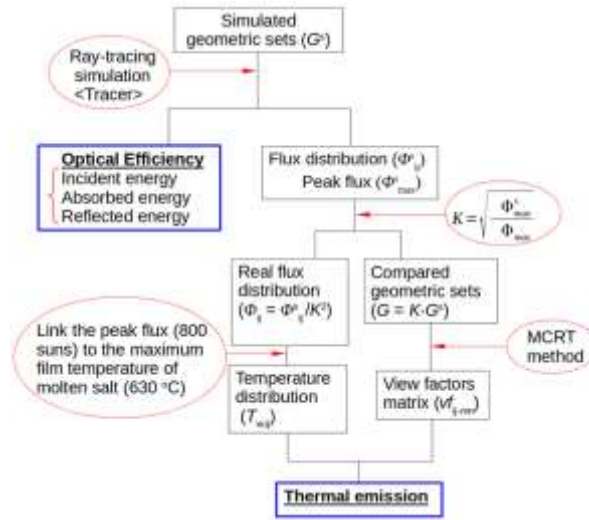
Figure 3. Investigation procedure

The definition of the field and ray-source in the simulation is same as the previous study (Wang et al., 2016). The structure of tubes is also not applied in this optical model, but will be considered in the future work. The absorptivity is set as 0.95 for all of the receiver surfaces studied here.

2.2. Thermal Model

The thermal efficiency evaluated in this study is defined in Eq.(12), in which the losses just include radiative thermal emission:

$$\eta_{th} = \frac{\dot{Q}_{emission}}{\dot{Q}_{abs}} \tag{12}$$

The overall receiver efficiency is defined as:

$$\eta_{rec} = \eta_{opt} \cdot \eta_{th} \tag{13}$$

The procedure for calculating the thermal emission are summarised in Figure 4. There is currently no feedback to accurately refine the external temperature.
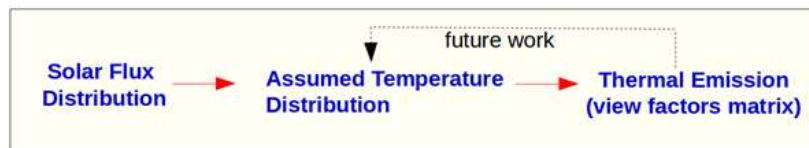
Figure 4.Procedure for calculating the thermal emission

The wall temperature of each element for the radiative thermal emission calculation is approximated basing on the flux distribution. The elements are same as those were used in the optical model. Energy balance can applied to the element as in Eq.(14), where conductive losses are neglected, convective coefficients are constant, radiation model is diffuse and grey surface with view factor of 1 to the environment, and the temperature of internal flow is the constant value of receiver inlet and outlet average temperature. The nomenclature of Eq.(14) and the constant value to be used are listed in Table 2.

$$\Phi_{ij} = \dot{q}_{conv,\text{inner},ij} + \dot{q}_{conv,loss,ij} + \dot{q}_{rad,loss,ij}$$
$$= h_i \cdot (T_{w,ij} - T_f) + h_o \cdot (T_{w,ij} - T_a) + \sigma \cdot \varepsilon \cdot (T_{w,ij}^4 - T_a^4) \tag{14}$$

The maximum film temperature for molten salt 630 °C (González et al.,2016) is assumed to occur at the same place as the peak flux (800 suns). Therefore, with the constants assumed in Table 2, the internal convection coefficient h_i can be calculated from Eq.(14), that is 3755 W/m²K. Then the temperature of the rest of the elements can be obtained by the corresponding flux.

Table 2. The nomenclature of Equation (14) and the constant values being used for the initial temperature calculation

|			
Φ_{ij}	The flux on element (i,j), obtained from optical model	σ	Stefan–Boltzmann constant, 5.67×10^{-8} W/(m²K⁴)
T_a	Ambient temperature, 25 °C	ε	Surface emissivity, 0.9
$T_{w,ij}$	Wall temperature of element (i,j), need to be obtained	h_o	The external convection coefficient, taken as constant, 10 W/(m²K)
T_f	Temperature of internal fluid, taken as the average: $(290+565)/2 =427.5$ °C	h_i	The internal convection coefficient, to link the peak flux with the maximum film temperature for molten salt

View factors are calculated for the section that constituted by the space and two adjacent blades. Because all of the blades are equal-area, the result can be reused for all the sections. The surfaces in the section are separated as the same number of elements as those in the optical model. The pair-wise view factor matrix can be obtained from MCRT method. With the view factor matrix and temperature distribution, thermal emission can be obtained accordingly (Bergman et al., 2011).

Actually, there would be an iterated process that substitutes the thermal emission obtained from the real view factors into Eq.(14) and then obtain a new temperature distribution and re-calculated the thermal emission, as the loop shown in Figure 4. But the iteration procedure has not yet been implemented for this study.

3. Results and Discussion

3.1. Flat Receiver

The size of the flat receiver is 10 m by 10 m. While changing the inclination angle, as shown in Figure 5(a), the absorbed energy increases slightly within 1% from 0° to 26.1° and decreases slowly till around 50°, and then dramatically drops down 25% at 90°. As to the peak flux, it is also the highest when the angle is 26.1°, the angle at which the normal of the

(a)   **(b)**
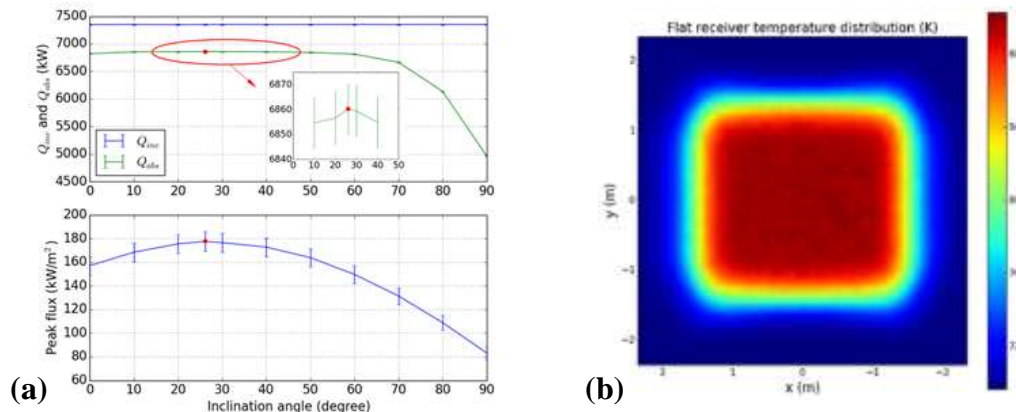
Figure 5. (a) Simulated flat receivers with different inclination angles; (b) Temperature distribution on the real flat receiver from the thermal model in Section 2.2

aperture plane points to the centre of the heliostat field. This is mainly due to a cosine effect on the aperture.

The inclination angle of 26.1° is chosen as the reference case to calculate the thermal performance and compare with bladed receivers because it has the maximum energy absorption.

Figure 5(b) shows the temperature distribution of the real flat receiver based on the thermal model (Section 2.2). The scaled dimension and efficiencies are listed in Table 3. The reflection is 5% because the surface absorptivity is set as 0.95. The thermal emission is 429.4 kW which accounts for 6.3% of the absorbed energy. The overall receiver efficiency is 87.5%.

Table 3. Performance of the simulated and the real flat receiver while the inclination angle is 26.1° (facing towards to the centre of the field)

Case	K_f	Size (m)	$\Phi_{f,max}$ (kW/m²)	Q_{in} (kW)	Q_{abs} (kW)	Q_{refl} (kW)	$Q_{emission}$ (kW)	η_{opt}	η_{th}	η_{rec}
Simulated	-	10	177.6	7349.8 ± 5	6860.2	361.1	-	93.3 %	-	-
Real	0.47	4.7	800	7349.8 ± 5	6860.2	361.1	429.43	93.3 %	93.7 %	87.5 %

3.2. Bladed Receiver

The optical and thermal performance of bladed receivers are investigated through varying number of blades (N), length of blade (B) and blade inclination angles (β and φ).

3.2.1. Blade Angles Study (β, φ)

Figure 6 shows the results for blade angles study, in which β and φ was defined in Figure 2, and the angle θ can be obtained by Eq.(10).
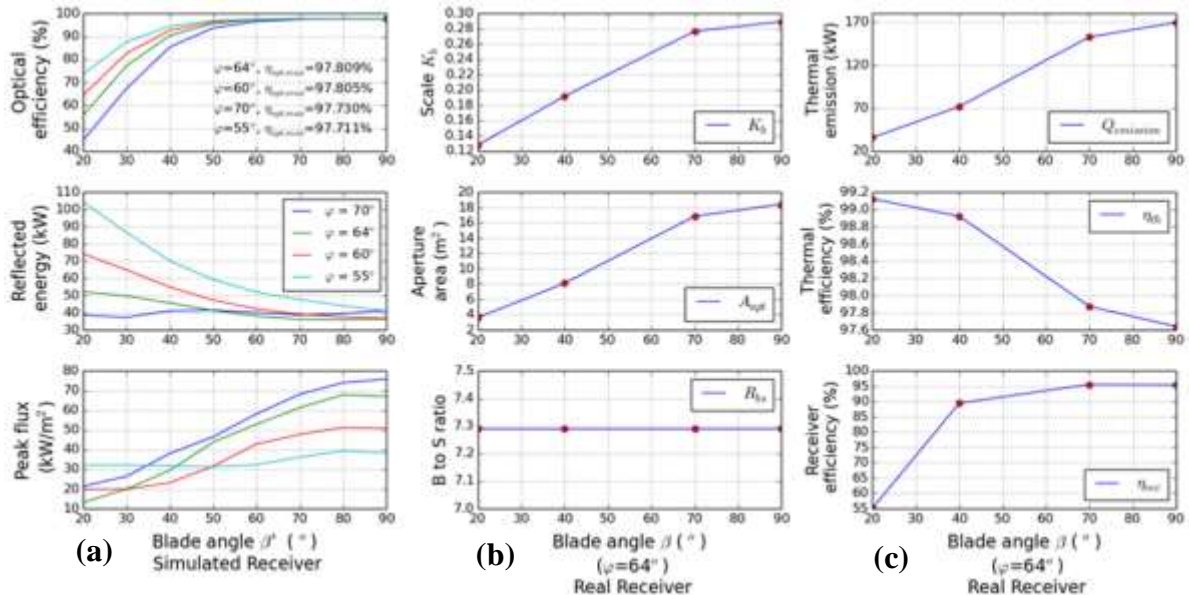
Figure 6. (a) Optical performance of the simulated receivers, the number and depth of blades are fixed as 25 and 3 m; (b) Geometrical parameters of the real receivers; (c)Thermal performance of the real receivers, the red spots are the calculated cases.

As shown in Figure 6(a), optical efficiency increases as the angle β going up. The best optical efficiency is when the blades perpendicular to the back wall (β=90°), in all of the cases of φ.

Among the four angles of φ, the best optical efficiency is at 64°, at which the blades are facing towards the centre of the field, although the differences are very small.

The peak flux shown in Figure 6(a) as well as those in the figures in the following sections is the peak flux in all area except the blade tips. This approach was chosen because the peak flux is the primary value to link molten salt film temperature. Only the main surfaces are considered, where the bulk of tubes will exist. The effect of the peak flux on tips will be discussed in Section 3.2.4.

It is interesting to notice that the trend of peak flux is increasing while angle β goes up, but the rate of increase slows when angle φ decreases. The angle φ indicates the direction that blades face towards to the field. At smaller φ, blades face to the nearer heliostats from the tower, and larger φ towards to the farther heliostats. One possible reason for this trend of peak flux shown in Figure 6(a) is that there are less heliostats near the tower than those far from the tower in the NSTTF field. Further simulations can be designed to test this hypothesis.

The angle $\varphi=64°$ is chosen for the thermal performance study. Because the view factor calculation is computationally expensive, four representative angle β are selected, as the red spots shown in Figure 6 (b) and (c).

When the angle β increases, the geometrical scale goes up with the peak flux rises, so the aperture area of the real bladed receivers is enlarged. While the aperture area goes up, the thermal emission increases and thermal efficiency decreases. The overall receiver efficiency is still showing an upward trend because it depends on both optical efficiency and thermal efficiency. The optical efficiency at $\beta=20°$ is just 40%, at which a big amount of spillage occurs (because θ becomes a negative value). In order to keep the same spillage level with the reference flat receiver, the inclination angle θ should be 26.1°. While $\beta=90°$ is selected for the following studies, because it has the best optical performance, φ will be 63.9° according to Eq.(10).

3.2.2. Blade Number Study (N)

Figure 7(a) shows the optical performance of the simulated bladed receiver with varying number of blades (N), while the depth of blade (B) is fixed as 3 m, angle β and φ are 90° and 63.9° respectively.
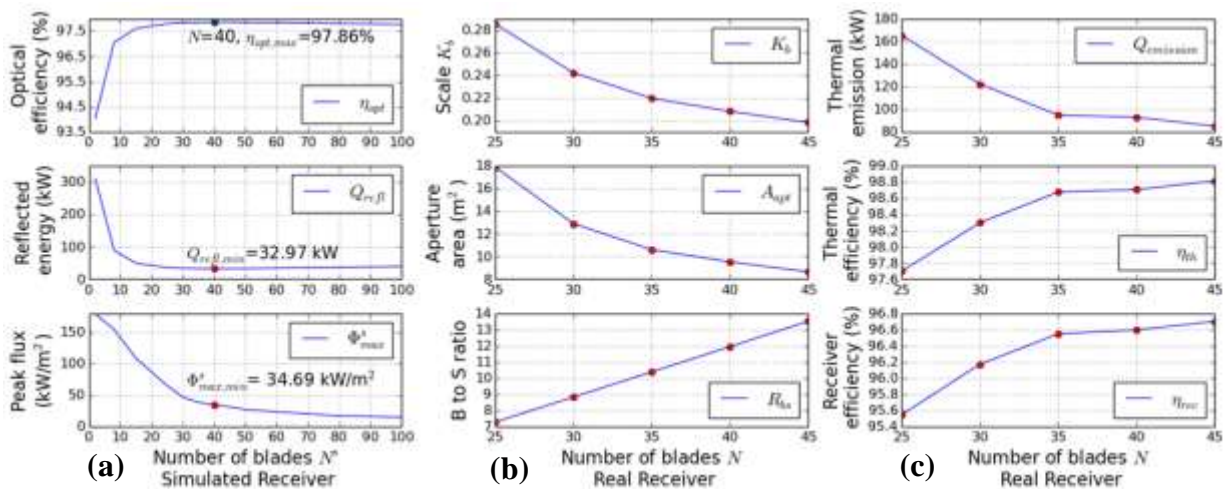
Figure 7. (a) Optical performance of the simulated receivers, with blade depth 3 m, angle β 90° and φ 63.9°; (b) Geometrical parameters of the real receivers; (c) Thermal performance of the real receivers, the red spots are the calculated cases.

Increasing from 2 to 20 blades, reflection decreases dramatically because the cavity-like shape of the spaces between blades improves light-trapping effect. While adding more blades improve light-trapping, it also results more reflection from blade tips and ends. The marginal effect becomes less significant when the number of blade larger than 30. The maximum optical efficiency is observed at 35 blades, although changes in optical efficiency are very small between 25-45 blades.

As shown in Figure 7(a), peak flux decreases as the number of blades increases. This is because the fact that while blades are added on the fixed size back wall, the space between the blades becomes smaller, and the blade depth (B) to space (S) ratio goes higher. The back wall, where most of the peak flux is observed, will be better shaded by the relatively 'longer' blades.

Blade numbers of 25, 30, 35, 40, 45 are selected for the thermal performance analysis, the results are shown in Figure 7 (b) and (c), where all of the cases have been scaled down to yield a constant value of peak flux compared with the real flat case as described in Fig.1. As the simulated peak flux goes down, the geometrical scale factor decrease. Adding blades will increase the blade depth to space ratio, but the aperture area, which is defined as:

$$A_{apert} = W \cdot H + 2W \cdot B + 2H \cdot B \tag{15}$$

would not be influenced by number of blades. The aperture area drops because the scale factor decreases, that makes W, H and B smaller. With the aperture area decreases, thermal emission goes down and thermal efficiency increases. For the overall receiver efficiency, the highest point is reaching to 96.7%. It is 9.2% higher than the reference flat receiver.

3.2.3. Blade Depth Study (B)

Figure 8(a) shows the optical performance of the simulated bladed receiver with varying depth of blades (B), while the number of blade (N) is fixed as 3 m, angle β and φ are 90° and 63.9° respectively.
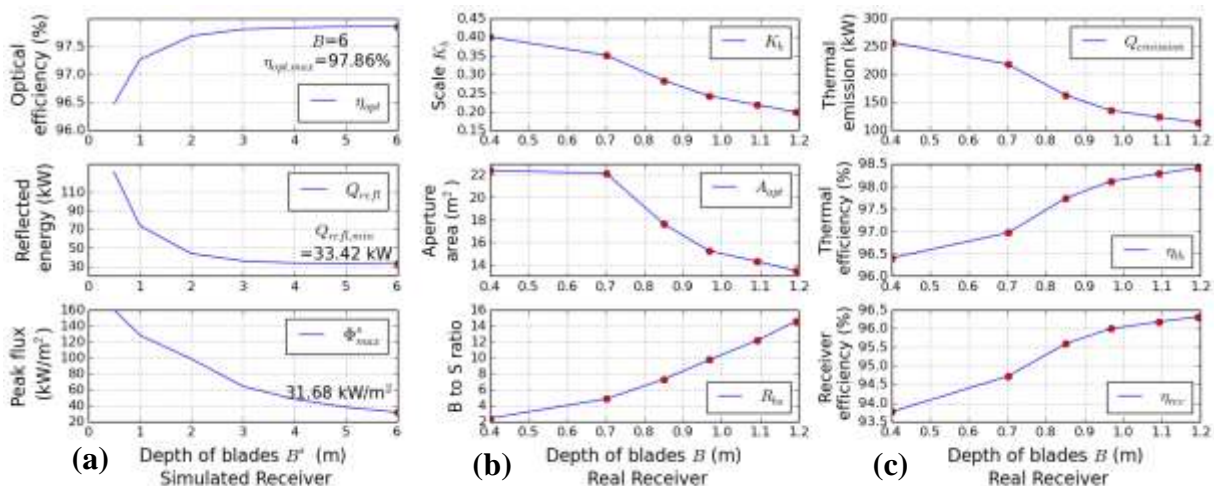
Figure 8. (a) Optical performance of the simulated receivers, with 25 number of blades, angle β 90° and φ 63.9°;(b) Geometrical parameters of the real receivers; (c) Thermal performance of the real receivers, the red spots are the cases be calculated, which are converted from simulated receivers with varying depth 1-6 m.

As shown in Figure 8, while the depth of blades increases, the B to S ratio increases, and correspondingly the optical efficiency goes up and peak flux goes down. It is due to the same

reasons that analysed in Section 3.2.2.

For the thermal performance, the selected real cases are converted from simulated bladed receivers with depth varying 1-6 m. The aperture area must be enlarged by the increasing depth, as shown in Eq.15. But the aperture area is decreasing here because the scale goes down, which leads to W and H both decrease. The overall effect (of increasing depth and decreasing back wall) makes the aperture area goes down. With the aperture area goes down, thermal emission goes down and thermal efficiency increases.

3.2.4. Real Receiver Comparison

Figure 9 is a summary of all of the real receivers be calculated. As discussed above, optical and thermal efficiency goes up with smaller aperture area. The aperture area is actually showing the concentration ratio that required from the heliostat field. An average concentration ratio on the receiver aperture can be defined as:

$$CR = \frac{Q_{inc}/A_{apert}}{DNI} \qquad (16)$$

Where DNI is the *Direct Normal Irradiance*, which is adopted as 1000 kW/m^2 here; the incident energy, Q_{inc}, is 7350 kW here for all of the cases been simulated, because the heliostat field is fixed. Therefore, the concentration ratio can be calculated by the aperture area for each case and be plotted in Figure 9.

(a)   (b)
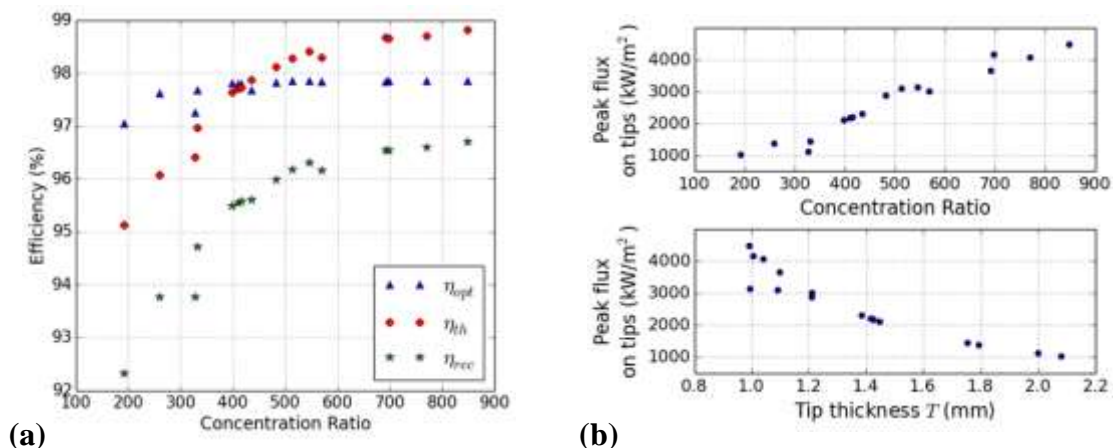
Figure 9. A summary of all of the real bladed receivers be calculated: (a) Efficiencies increase as CR increases; (b) Peak flux on tips rises up when CR goes higher

As shown in Figure 9(a), optical efficiency and thermal efficiency is going up while the concentration ratio increases. This demonstrates that smaller aperture with higher concentration ratio can catch more reflection and re-radiation, which is the same conclusion that was drawn in the first-order analysis on the relation between concentration ratio and efficiency (Pye et al., 2016).

With the same incident energy and peak flux constraints, bladed receiver can be made much smaller. The highest concentration ratio among the cases be calculated is 845, where the thermal efficiency can reach to 98.3%, and with the optical efficiency of 97.9%, the overall bladed receiver efficiency can be 96.7%. The overall efficiency is increased 9.2% compare to the reference flat receiver.

Under higher concentration ratio, the peak flux on the tips will also rise up. As shown in Figure 9(b), the highest peak flux on tips can be 4 to 5 times higher than that of the bulk of

tubes (800 suns). This high flux will easily case thermal damage. However, this results are obtained by setting the absorptivity of tips also as 0.95. Coating of low absorptivity and high-temperature tolerance (eg. white ceramic) is expected to protect the blade tip regions. Varying absorptivity and thickness of tips will be investigated in further studies.

4.   Conclusion

The optical and thermal performance are evaluated for a flat receiver and bladed receivers with a range of different sizes. Under the constraints of same peak flux and same incident energy, bladed receiver with smaller aperture and higher concentration ratio can catch more reflection and re-radiations, which is same as the conclusion that was drawn in the first-order analysis on the relation between concentration ratio and efficiency (Pye et al., 2016), but with a detailed analysis of flux distribution.

Among all of the cases that have been studied, when concentration ratio reaches 845, the overall receiver efficiency can be improved by 9.2%, when compared to the reference flat receiver. It seems that if the concentration ratio goes higher, the performance of the bladed receiver will keep being improved. What is the highest concentration ratio can be achieved when considering both the bladed receiver and heliostat field designs? It will be an interesting topic for future work.

References

Bergman, T. L.,Lavine, A. S.,Incropera, F. P., Dewitt, D. P.,'Fundamentals of heat and mass transfer',7th Edition

Falcone,P. K., 1986, 'A handbook for Solar Central Receiver Design', *Sandia Report SAND86-8009*. Sandia National Laboratories, Albuquerque, NM

González,A. S., Sánchez M.R.R., Santana D.,2016, 'Aiming strategy model based on allowable flux densities for molten salt central receivers',*Solar Energy*

Ho, C.K., Iverson, B.D., 2014,'Review of high-temperature central receiver designs for concentrating solar power',*Renewable and Sustainable Energy Review*,

Kolb,G. J., 2011, 'An Evaluation of Possible Next-Generation High-Temperature Molten-Salt Power Towers',*Sandia Report SAND2011-9320*, Sandia National Laboratories

Pye, J., Coventry, J.,Ho, C., Yellowhair, J., Nock, I., Wang, Y., Abbasi, E., Christian, J., Ortega, J. and Hughes, G., 2016. 'Optical and Thermal Performance of Bladed Receivers', *SolarPACES*

Wang, Y., Asselineau, C.A., Coventry, J., and Pye, J., 2016, 'Optical performance of bladed receivers for CSP systems', *Proceedings of the ASME 2016 Power and Energy Conference*

Yellowhair, J., Christian, J. M.,and Ho, C. K., 2014, 'Evaluation of solar optical modeling tools for modelingcomplex receiver geometries', I*n Proceedings of the ASME2014 8th International Conference on Energy Sustainability*,Boston, Massachusetts, July, 2014